Nikon BioImaging Lab

Let us do the imaging for you.

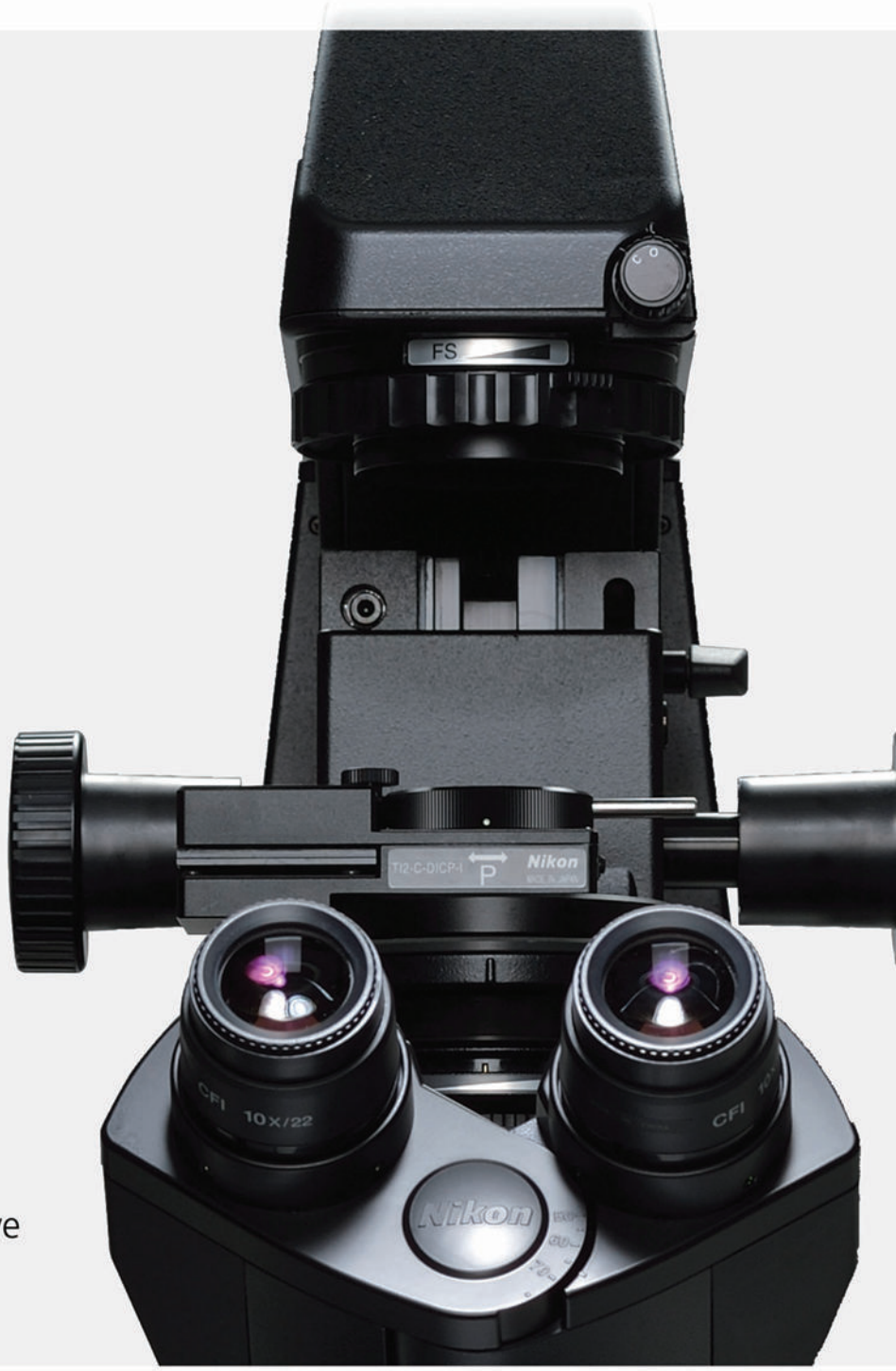

The Nikon BioImaging Lab is a state-of-the-art facility located in Cambridge, Massachusetts, that provides advanced technologies to support the burgeoning regenerative medicine and biotech sector.

For more information, visit www.microscope.healthcare.nikon.com/bioimaging-lab

Nikon Instruments Inc. ■ www.microscope.healthcare.nikon.com ■ nikoninstruments@nikon.net

STEM CELLS®

TISSUE-SPECIFIC STEM CELLS

HPRT and Purine Salvaging Are Critical for Hematopoietic Stem Cell Function

MONA VOGEL,[a] BETTINA MOEHRLE,[a] ANDREAS BROWN,[a] KARINA EIWEN,[a] VADIM SAKK,[a] HARTMUT GEIGER[a,b]

Key Words. Hematopoietic stem and progenitor cells (HSPCs) • Purine nucleotide metabolism • HPRT-associated purine salvaging • Proliferation kinetics • Mitochondria function

[a]Institute of Molecular Medicine, Ulm University, Ulm, Germany; [b]Division of Experimental Hematology and Cancer Biology, Cincinnati Children's Hospital Medical Center and University of Cincinnati, Cincinnati, Ohio, USA

Correspondence: Hartmut Geiger, Ph.D., Institute of Molecular Medicine and Stem Cell Aging, Ulm University, James Franck Ring 11c, 89081 Ulm, Germany and Cincinnati Children's Hospital Medical Center, Cincinnati, Ohio 45229, USA. Telephone: 1-513-636-1338 or 49-731-500-57650. e-mail: hartmut.geiger@uni-ulm.de

Received April 24, 2019; accepted for publication August 23, 2019; first published online October 1, 2019.

http://dx.doi.org/10.1002/stem.3087

ABSTRACT

Adult hematopoietic stem cells (HSCs) maintain tissue homeostasis and regenerative capacity of the hematopoietic system through self-renewal and differentiation. Metabolism is recognized as an important regulatory entity controlling stem cells. As purine nucleotides are essential for metabolic functions, we analyzed the role of hypoxanthine guanine phosphoribosyl transferase (HPRT)-associated purine salvaging in HSCs. Here, we demonstrate that hematopoietic stem and progenitor cells (HSPCs) show a strong dependence on HPRT-associated purine salvaging. HSPCs with lower HPRT activity had a severely reduced competitive repopulation ability upon transplantation. Strikingly, HPRT deficiency resulted in altered cell-cycle progression, proliferation kinetics and mitochondrial membrane potential primarily in the HSC compartment, whereas more committed progenitors were less affected. Our data thus imply a unique and important role of HPRT and the purine salvage pathway for HSC function. STEM CELLS *2019;37:1606–1614*

SIGNIFICANCE STATEMENT

Metabolism controls stem cell function. Purine metabolism is a critical component of cellular metabolism. This article reports that a reduced activity of the purine salvaging enzyme HPRT in HSCs ($HPRT^{low}$ HSCs) results in reduced fitness of HSCs and alters their cell-cycle profile and the function of their mitochondria. The data obtained suggest that this phenotype of $HPRT^{low}$ HSCs is due to elevated levels of purine degradation rather than a lack of purine recycling, implying an important role for HPRT-mediated purine salvaging for HSC function.

INTRODUCTION

Hematopoietic stem cells (HSCs) are able to self-renew and differentiate into all blood cell lineages to maintain homeostasis and regeneration. Metabolism has emerged as an important regulatory entity influencing the function and the potential of HSCs [1]. HSCs are primarily quiescent and show low mitochondrial activation and function but high levels of glycolysis [2–5]. Upon stress like for example blood loss, HSCs switch to oxidative phosphorylation to enter the cell cycle to undergo self-renewal and differentiation [6]. Recently, the activation of the purine nucleotide metabolism in HSCs could be linked to HSCs activation in response to stress [7]. Because purine nucleotides are not only direct components of DNA and RNA but as they are actually involved in almost all metabolic processes, they might be critical for both quiescent as well as proliferating cells.

Cells obtain purine nucleotides via either de novo synthesis or salvaging of free purine bases (aka recycling) [8] (Fig. 1A). These pathways differ in terms of energy consumption: The de novo synthesis of ATP and GTP requires an energy equivalent provided by the hydrolysis of 10 ATP molecules, yet, the purine salvage pathway only requires six ATP units [9]. Most organ systems and several cell lines prefer the salvage pathway [10, 11]; and thus recycling. An increase of de novo synthesis is usually observed during cell growth and proliferation and upon malignant transformation [10, 12, 13]. Amidophosphoribosyltransferase (PPAT) catalyzes the first and rate limiting step of de novo synthesis in which 5′-phosphoribosyl-1-pyrophosphate (PRPP) serves as the starting substrate. Free purine bases can be recycled by hypoxanthine guanine phosphoribosyl transferase (HPRT, guanine and hypoxanthine) and adenine phosphoribosyltransferase (APRT, adenine), or they can be degraded to uric acid by xanthine oxidase.

HPRT is ubiquitously expressed and catalyzes the conversion of hypoxanthine to IMP and guanine to GMP via transfer of the 5-phosphoribosyl

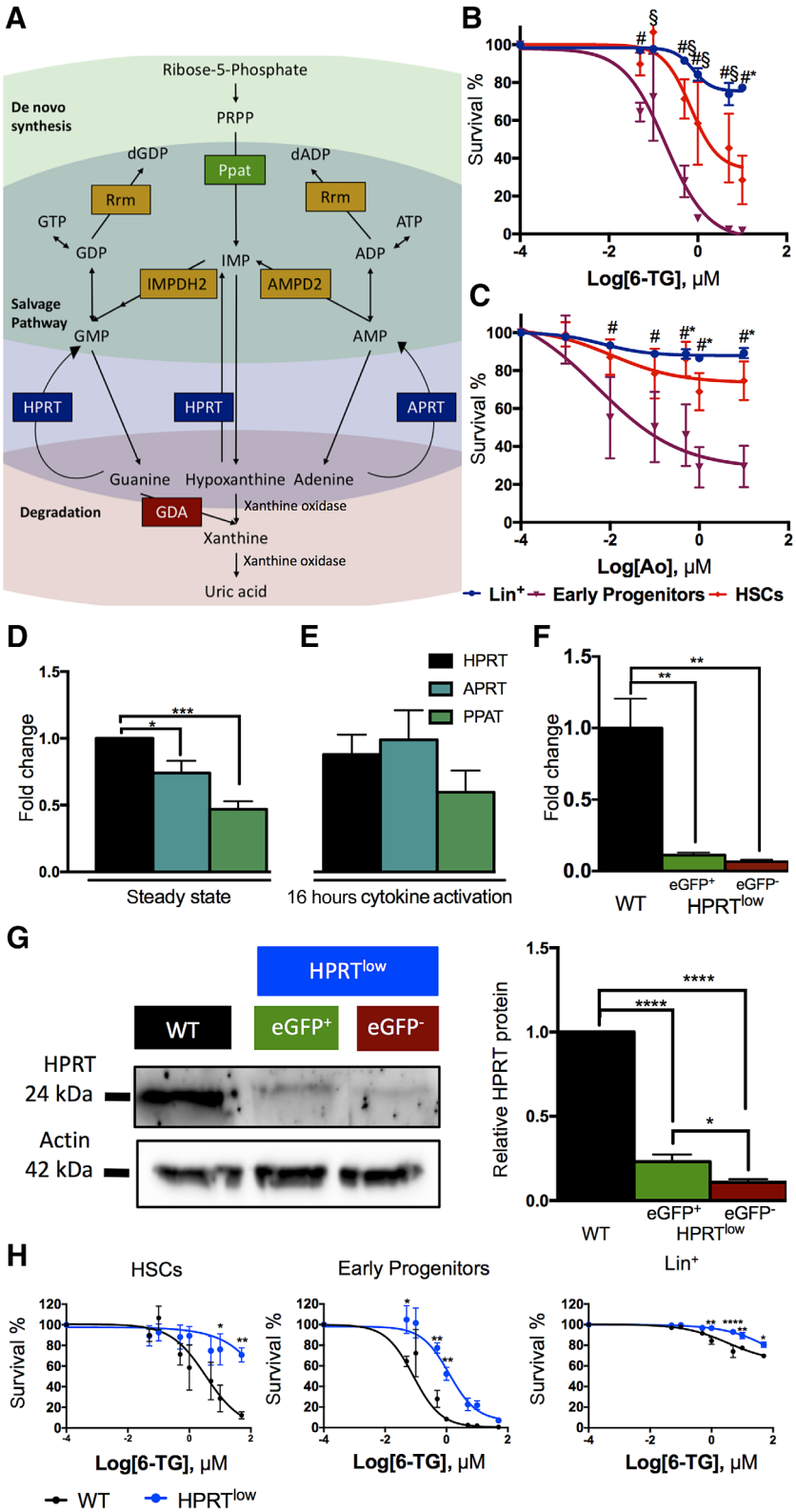

Figure 1. Hematopoietic stem cells (HSCs) relay on purine salvaging. **(A):** Simplified scheme of purine nucleotide metabolism. Green = steps in de novo synthesis; blue = steps in salvage pathway; red = steps in degradation of purine nucleotides; overlapping green/blue = de novo synthesis or salvage pathway; overlapping red/green = purines are degraded or salvaged. Analyzed enzymes are marked in the same color, yellow = both de novo synthesis or salvage pathway. Abbreviations: Gda, guanine deaminase; Impdh2, inosine monophosphate dehydrogenase 2; Ampd2, adenosine monophosphate deaminase 2; Rrm2, ribonucleotide reductase regulatory subunit M2. **(B, C):** Survival curve of different bone marrow (BM) populations from C57BL/6 mice after treatment with different dosages of (B) 6-TG or (C) Ao. Normalized 0 µM = 100%

(Figure legend continues on next page.)

group from PRPP [14]. APRT converts adenine in the same manner. The *hprt1* gene is located on the X-chromosome and highly conserved between mice and humans [15]. Partial HPRT deficiency results in gouty arthritis, whereas an almost complete deficiency leads to the Lesch–Nyhan disease. The latter is characterized by severe neurological dysfunction in addition to gouty arthritis, including retardation, choreoathetosis, and aggressive and compulsive self-mutilation. Whether there are HSC phenotypes in these diseases have not been investigated in detail.

Bone marrow (BM) cells express low levels of *Ppat* and high levels of *Hprt* [14]. HSCs show the highest level of HPRT expression right after active CD8 positive T-cells [16] which might imply a critical role of HPRT-driven purine salvaging for HSCs. In this study, we demonstrate that a reduced level and activity of HPRT, which results in impaired purine salvaging in HSCs, resulted in a reduced function of HSCs. Additionally, HSCs with reduced levels of HPRT were altered in cell-cycle progression, proliferation kinetics, and mitochondrial function, whereas hematopoietic progenitors were only marginally affected. Our data reveal that HSCs strongly depend on HPRT-associated purine salvaging to maintain the function and the potential of HSCs.

Materials and Methods

Mice

C57BL/6J mice were obtained from Janvier (Le Genest-Saint-Isle, France) or from our on-site breeding cohort (based on C57BL/6 animals from Janvier). Breeding pairs for B6.SJL-Ptprc<a>Pepc<b>/BoyJ recipient mice were obtained from Charles River (Wilmington, MA, USA). The $HPRT^{low}$ mouse model (B6xB6 Tgh (EGFP) Brl (−/−)) was kindly provided by Klaus Schwarz, and the HPRT knockout mice were a gift from Erich Schneider. All mice were bred and housed under specific pathogen-free conditions at the Tierforschungszentrum of Ulm University. The experiments were performed in compliance with the German Law for Welfare of Laboratory Animals and were approved by the Regierungspräsidium Tübingen (TVA). For $HPRT^{low}$ mice, peripheral blood (PB) smears from male mice were analyzed for the transgene by fluorescence microscopy using a GFP fluorescence filter. Only male mice were used in the experiments.

Reagents and Standard Procedures

Hanks' balanced salt solution (HBSS) (BioWhittaker Lonza, Basel, Switzerland) and Iscove's Modified Dulbecco's Medium (IMDM) (BioWhittaker Lonza) were supplemented with 10% fetal bovine serum (FBS) (Hy-Clone Fetal bovine serum defined; Thermo Scientific, Waltham, MA, USA) and 1% penicillin/streptomycin if not otherwise specified. Femora, tibiae, and hip bones were flushed to obtain total BM. If needed, mononuclear cells (LDBM) were isolated by low density centrifugation (26 minutes, RT, no brake/acceleration) on Histopaque-1083 (Sigma-Aldrich, St. Louis, MO, USA). If not otherwise described, LDBM cells were directly used for experiments (steady state) and partly were in vitro stimulated with cytokines for 48 hours (37°C, 21% O_2 and 5% CO_2 in IMDM +1% GlutaMax (Gibco, Thermo Scientific) + 50 ng/ml murine SCF (Prospec-ProteinSpecialists, Rechovot, Israel) + 100 ng/ml Flt-3 (Prospec-ProteinSpecialists) + 100 ng/ml TPO (Prospec-ProteinSpecialists) (Stimulated state).

Hematopoietic Progenitor Cell Staining

To LDBM cells, biotin-labeled lineage-antibody cocktail was added (Table S1) or LDBM was lineage depleted by using a mouse lineage depletion kit (Miltenyi Biotec, Bergisch Gladbach, Germany) according to the manufacturer's protocol with the following adaptions: we used 20 µl/10^7 cells of the beads and cells were resuspended at a concentration of 3 ml/10^7 cells. After washing, FC-Block anti-mouse CD16/CD32 Clone 93 (eBioscience, CA, USA) was added. For the staining, Streptavidin, anti-CD34, anti-Sca-1, and anti c-Kit were added for 1 hour at 4°C in the dark (Table S1).

Quantitative Real-Time PCR

Total RNA was isolated either from FACS (Aria III, BD Biosciences, Franklin Lakes, NJ, USA) sorted HSPCs or $eGFP^+$ and $eGFP^-$ LDBM cells using the RNeasy Micro-Kit (Qiagen, Hilden, Germany). HSPCs cells were processed either directly after sorting (steady state) or after 16 hours stimulation. in vitro stimulation of HSPCs was induced by a 16 hours incubation at 37°C, 21% O_2 and 5% CO_2 in IMDM +1% GlutaMax + 50 ng/ml murine SCF + 100 ng/ml Flt-3 + 100 ng/ml TPO. A maximum of 500 ng of RNA was used for cDNA synthesis (QuantiTect Reverse Transcription Kit; Quiagen). Normalization was made with Gapdh and fold change was calculated by ΔΔCt (Delta delta Ct) method, in which wild type (WT) or HPRT were used as baseline (=1), for more details see supplement.

Western Blot

In all, 5×10^5 LDBM cells were used for protein extraction. Anti-mouse actin antibody (clone: AC-15, Sigma-Aldrich, 1:1,000) was used to identify actin. The strength of the actin signal was used to normalize for differences in gel loading. Anti-rabbit HPRT clone: FL-218 (SantaCruz Biotechnology, Dallas, TX, USA) for the target (1:200). Secondary antibodies donkey anti-mouse IG-HRP sc-2314 and donkey anti-rabbit IG-HRP sc-2077 were added at 1:10,000. Band intensities were quantified with ImageJ software.

(Figure legend continued from previous page.)
alive. Curve fitting with prism nonlinear fit: log(inhibitor) vs. response variable slope (n = 3–5 [2–3 mice/n]; two-way ANOVA #$p \le .05$ between Lin^+ and early progenitor cells; *, $p \le .05$ between Lin^+ and HSCs; $^{\S}p \le .05$ between early progenitor cells and HSCs). **(D, E):** mRNA expression of C57BL/6 hematopoietic stem and progenitor cells (HSPCs) of the indicated genes (D) steady state (E) in vitro cytokine stimulation for 16 hours. Normalization with Gapdh (n = 3 [3 mice pooled/experiment]; unpaired t test *, $p \le .05$; **, $p \le .01$). **(F):** Expression of *Hprt* mRNA in C57BL/6 (WT), $HPRT^{low}$ $eGFP^+$, and $HPRT^{low}$ $eGFP^-$ LDBM cells (n = 3; one-way ANOVA **, $p \le .01$). **(G):** Western analysis of protein from WT, $HPRT^{low}$ $eGFP^+$, and $HPRT^{low}$ $eGFP^-$ LDBM cells. Left: representative western blot, HPRT with approximately 24 kDa and Actin as loading control with 42 kDa; right: quantification of band intensity normalized to the corresponding actin band (n = 3; one-way ANOVA *, $p \le .05$; ****, $p < .0001$). **(H):** Survival rates between WT and $HPRT^{low}$ BM populations after treatment with different dosages of 6-TG (n = 3–5 [2–3 mice pooled/experiment]; two-way ANOVA *, $p \le .05$; **, $p \le .01$; ****, $p < .0001$).

6-Thioguanin (6-TG) and Aminopterin (Ao) Survival Assay

LDBM cells were incubated for 48 hours with different dosages of 6-TG (Sigma-Aldrich) or Ao (Sigma-Aldrich). Conditions: 37°C, 21% O_2, 5% CO_2 in IMDM +1x GlutaMax + 50 ng/ml murine Stem Cell Factor + 10 ng/ml Interleukin-3 mouse (Prospec-ProteinSpecialists) + 100 ng/ml Interleukine-11 mouse (Prospec-ProteinSpecialists) + 100 ng/ml Flt-3 for Ao treatment additionally 16 μM Thymidine (Sigma-Aldrich) was added. Used dosages ranges of 6-TG or Ao were: 0.05–50 μM and 0.0001–10 μM. Afterward LDBM cells were stained with antibodies to define hematopoietic stem and progenitor cells. Before samples were analyzed by a BD LSR II, Propidium iodide (PI) (1 μg/ml) (Sigma-Aldrich) was added for live/dead staining. The survival rate was calculated by subtracting the percentage of PI^+ cells. Normalization was performed using 0 μM 6-TG/Ao = 100% alive cells. Curve fitting was performed with the software suite Prism 7.0 and a nonlinear fit: log(inhibitor) versus response variable slope.

Staining of PB and Total BM

PB was collected by cardiac puncture after euthanizing mice with CO_2 or in case of transplantation experiments from the facial vein. Total BM was collected by flushing femora, tibiae, and hip bones. Staining was performed with anti-CD3e, anti-B220, anti-Gr-1, and anti-Mac-1. For transplanted animals, anti-Ly5.2 and anti-Ly5.1 were used to identify donor and recipient cells. Red cell lysis was performed and cells were analyzed on a LSR II flow cytometer (BD Bioscience). Data are plotted as the percentage of B-cells ($B220^+$), T-cells ($CD3^+$), and myeloid ($Gr\text{-}1^+$, $Mac\text{-}1^+$ and $Gr\text{-}1^+$, $Mac\text{-}1^+$) cells among donor-derived $Ly5.2^+$ cells regarding transplantation experiment or among total white blood cells (antibodies Table S1).

Transplantation

Hematopoietic progenitor cell staining was performed on lineage depleted WT or $HPRT^{low}$ Ly5.2 cells. HSPCs were subsequently sorted on a FACS (Aria III, BD Biosciences) and kept overnight at 37°C, 5% CO_2, 3% O_2 in IMDM. The next morning 1,000 LSK (Ly5.2) along with 3×10^5 freshly prepared total BM competitor cells (Ly5.1) were transplanted into the tail vein of each lethally irradiated (7 + 4 Gy) mouse. Ly5.2/Ly5.1 chimerism in PB was monitored every 4 weeks. At least 20 weeks after transplantation, early hematopoiesis/total BM and PB staining was performed.

Cell-Cycle Analysis

Staining was performed with the BrdU flow kit (BD Pharmingen) as described previously [17].

Single-Cell Proliferation Kinetics

Terasaki plates (Greiner Bio one, Kremsmuester, Austria) were prepared by adding 20 μl of IMDM +10% FBS + 1% 100X Penicillin/Streptomycin +100 ng/ml murine SCF + 100 ng/ml G-CSF + 100 ng/ml TPO (all Prospec-ProteinSpecialists). HSCs were sorted into Terasaki plates, one single HSC in each well. After 1 hour, the count of correctly filled wells was determined. Terasaki plates were incubated for 48 hours at 3% O_2, 5% CO_2 and 37°C. Cell division was observed every 4–8 hours. For first division, all wells were counted with at least two cells.

TMRM and MitoSox

First, hematopoietic progenitor cell antibody panel staining was performed on LDBM cells. After staining, 50 nM TMRM (Invitrogen, Carlsbad, CA, USA) or 5 μM of MitoSox (Invitrogen) were added. Samples were incubated for 30 minutes at 37°C + vortex in the dark and washed with HBSS. Samples were measured by a BD LSRFortessa flow cytometer (BD Bioscience). Data are represented as fold change, calculated by dividing mean TMRM fluorescence measured in $HPRT^{low}$ cells through the mean TMRM fluorescence from the WT cells (three mice/*n*, WT and $HPRT^{low}$ cells were treated the same and measured in the same experiment).

ATP and ADP Amounts

Hematopoietic progenitor staining on lineage depleted cells was performed. Lin^+ cells were washed out of the lineage depletion kit column (Miltenyi Biotec). HSCs and early progenitor cells were sorted by FACS (Aria III, BD Biosciences) and either used directly after sort or cells were stimulated for 16 hours before performing ATP/ADP measurement (Sigma-Aldrich). For the ATP/ADP ratio, assay cells were washed (PBS) and resuspended at a concentration of 10^5/ml PBS, final 1,000 cells/well. Protocol of ATP/ADP ratio kit was followed, exception: ATP reagent was added to the wells and a background measurement was performed before adding the cell extract. Relative luminescence units were measured with standard luminescence on a Paradigm Detection Platform (Beckman Coulter, Brea, CA, USA). Data are plotted as fold change (see also analysis TMRM above).

Annexin V

Hematopoietic progenitor cell staining was performed with LDBM cells. Afterward, 5 μl of Anti-Annexin V antibody (BD Pharmingen) dissolved in 200 μl of Annexin V binding buffer was applied for 20 minutes at RT in the dark. Before analyzing by BD LSRFortessa (BD Bioscience), PI live/dead staining was used.

Data Analysis and Statistics

Data were assumed to meet normal distribution. If not otherwise stated data are displayed as means +1SEM. All statistical analyses were performed with the Graph Pad Prism 7 Software Suite. Correction for multiple comparison was performed using Sidak or Tukey Test (ANOVA) or Holm-Sidak method (*t* test). The number of biological repeats (*n*) is listed in figure legends.

RESULTS

HSPCs Depend on Purine Salvaging

We first determined the level of expression of the key players linked to the two pathways of purine metabolism. A general overview on the purine metabolism pathway is provided in Figure 1A, whereas gating strategies to define the distinct hematopoietic cell populations are illustrated in Figure S1. We then identify the relative enzymatic activity of the HPRT-driven salvage pathway versus the de novo synthesis in primitive hematopoietic cells using pharmacological suicide assays. Cells are killed by 6-thioguanine (6-TG) when it is metabolized by HPRT. Ao is a folate metabolism inhibitor that reduces nutrients for purine de novo synthesis. Cell death in response to Ao is thus an indication of the activity of purine de novo synthesis. HSCs were quite

sensitive to 6-TG with a survival rate of only 30% at a 10 μM concentration (Fig. 1B), whereas sensitivity to Ao was moderate, with more than 75% of cells surviving at a concentration of 10 μM (Fig. 1C). These data imply that HSCs primarily use the HPRT-dependent purine salvage pathway. Interestingly, early hematopoietic progenitor cells showed significantly reduced survival in response to both drugs, implying that early progenitors and thus cells that are only slightly more differentiated than HSCs use in addition to the salvage pathway also purine de novo synthesis (Fig. 1B, 1C). Interestingly, differentiated cells (Lin^+) exhibited the highest level of cells surviving both treatments, which implies a low need for purines in differentiated cells or they use pathways independent of HPRT and PPAT (Fig. 1B, 1C). As already implied previously [16], *Hprt* mRNA expression in HSPCs (LSK cells) was slightly elevated compared with the expression of both *Ppat* and *Aprt* in steady state (Fig. 1D), but similar upon activation by cytokines (Fig. 1E), demonstrating that the expression level of these genes might not be linked to the distinct usage of these pathways in primitive hematopoietic cells.

To further investigate the role of HPRT-mediated purine salvaging for HSCs, we analyzed hematopoietic cells from a novel mouse strain in which the level of expression of HPRT is significantly reduced compared with the expression in WT control animals ($HPRT^{low}$ animals). In this strain, an eGFP cassette was inserted at the *hprt1* gene locus under the control of the human elongation factor-1α promotor (Fig. S2A). Due to mechanisms currently not understood, only approximately 80% of all types of blood cells express eGFP in these hemizygous mice, translating into $eGFP^+$ and $eGFP^-$ hematopoietic cells (Fig. S2B). The integration of this cassette resulted in reduced levels of HPRT, both with respect to RNA (Fig. 1F) and protein (Fig. 1G). Interestingly, $eGFP^+$ hematopoietic cells, in comparison with $eGFP^-$ cells, presented with a slightly higher but still overall low level of expression of HPRT, generating a system with graded levels of reduction of HPRT levels in hematopoietic cells. To confirm also the loss of HPRT activity in hematopoietic cells from these animals, a 6-TG assay was performed (Fig. 1H). HSCs, early progenitors, and Lin^+ cells showed, compared with control cells, increased survival in response to 6-TG, confirming reduced activity of HPRT and thus reducing activity of the purine salvage pathway in hematopoietic cells from $HPRT^{low}$ mice.

Hematopoietic Cells Do Not Elevate Purine De Novo Synthesis to Compensate for the Loss of Purine Salvaging

We then asked whether primitive hematopoietic cells might increase de novo synthesis of purines in case of the compromised purine salvaging pathway. To this end, we first determined the level of expression of purine metabolism-related enzymes in WT and $HPRT^{low}$ HSPCs in steady state as well as after stimulation with cytokines for 16 hours (Fig. 2A, 2B). In general, there were only none or minor differences in the level of expression of enzymes linked to the de novo synthesis or the APRT-associated salvage pathway (like Ppat, Rrm, Impdh2, Ampd2, Aprt) in either steady state or after stimulation (Fig. 2A, 2B). Thus, low levels of HPRT do not result in compensatory changes in expression of genes in the purine metabolism pathway. We next tested whether $HPRT^{low}$ HSCs and early progenitors might be more susceptible to killing induced by Ao, which might imply an increase in the activity of the de novo synthesis pathway. Interestingly, HSCs, early progenitors and

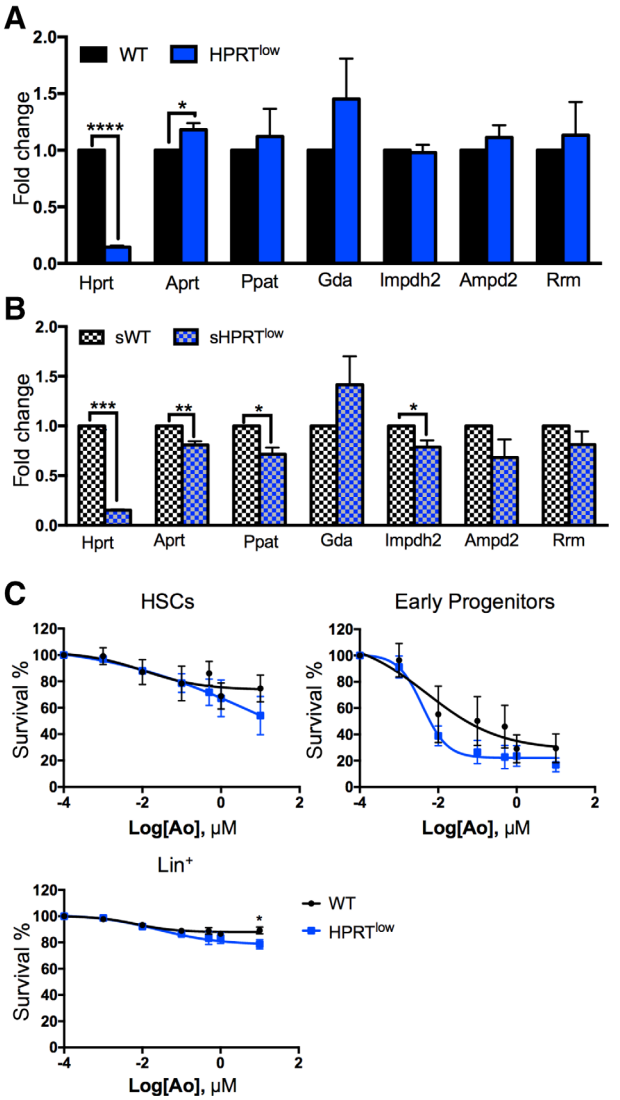

Figure 2. Hematopoietic stem and progenitor cells (HSPCs) do not elevate de novo synthesis to compensate for the loss of purine salvaging. **(A, B):** Gene expression patterns of important purine nucleotide enzymes. mRNA was isolated from (A) freshly sorted or (B) 16 hours in vitro stimulated HSPCs of wild-type (WT) or $HPRT^{low}$ mice. RT-PCR was performed, normalization took place with Gapdh (n = 3 [pooled 3 mice/experiment]; unpaired t test *, $p \le .05$; **; $p \le .01$; ****, $p < .0001$). **(C):** Survival curve of different BM populations from WT or $HPRT^{low}$ mice after treatment with different dosages of Ao in vitro. Normalized 0 μM = 100% alive. Curve fitting with prism nonlinear fit: log(inhibitor) vs. response variable slope. Curves are shown for hematopoietic stem cells (HSCs), early progenitors and mature (Lin^+) cells (n = 5 [pooled 2–3 mice/experiment]; two-way ANOVA).

Lin^+ cells from $HPRT^{low}$ mice presented with survival curves in response to Ao that were almost identical to the ones from WT cells (Fig. 2C). Hematopoietic cells with reduced activity of HPRT and thus an impaired purine salvage pathway (Fig. 1H) do not elevate purine de novo synthesis in a significant manner.

$HPRT^{low}$ HSCs Show Impaired Engraftment

To examine the influence of reduced HPRT activity and thus impaired purine salvaging on the function of HSCs, we

performed competitive transplantation assays and monitored donor chimerism in PB for at least 20 weeks post-transplant as an indicator for the function of transplanted HSCs (Fig. 3A). Both chimerism in PB driven by transplanted eGFP$^+$ or eGFP$^-$ HPRT^{low} HSCs was strongly reduced in comparison to chimerism supported by transplanted WT cells (Fig. 3B). HPRT^{low} and WT HSPCs maintained a similar differentiation potential as determined by their relative contribution to myeloid and lymphoid (T- and B-) cells (Fig. 3C). eGFP$^-$ cells, showing the lowest level of HPRT expression, also showed the lowest percentage of contribution to PB (Fig. 3B). Mirroring the reduced chimerism in blood, the frequency of both HPRT^{low} eGFP$^-$ or GFP$^+$ derived HSCs and the number of more committed progenitor and differentiated cells (early progenitors, LK, and BM cells) was also reduced in the BM of recipients (Fig. 3D). Upon secondary transplantation, the percentage of HPRT^{low} donor-derived cells in PB was further reduced. HPRT^{low} eGFP$^-$ derived cells were not able to engraft at all whereas HPRT^{low} eGFP$^+$ derived cells were further reduced compared with the percentage shown in primary transplants; however, engraftment was constant over time (Fig. S3). Similarly, transplantation of HPRT knockout HSPCs also resulted in overall reduced engraftment in PB without a skewing in differentiation (Fig. S4).

In strong contrast though, HPRT^{low} mice presented with normal hematopoietic parameters in steady state. The frequency of B-, T-, and myeloid cells in both PB (Fig. 3E) and BM (Fig. 3F) and the frequency of HSC as well as early progenitor cells in BM (Fig. 3G) were similar in WT and HPRT^{low} mice. HPRT^{low} mice presented with a small but significant reduction in the red blood cell count among all the red cell blood parameters determined (Fig. 3H). These data imply that impaired purine salvaging results in a reduced function of HSPCs upon stress or activation like transplantation, but interestingly not in steady-state hematopoiesis.

HPRT^{low} HSCs Manifest with Changes in Proliferation Kinetics and Reduced Mitochondrial Activity

To further investigate likely mechanisms for the reduced level of engraftment of HPRT^{low} HSPCs, we determined cell-cycle distribution, proliferation kinetics, and the level of apoptosis in primitive hematopoietic cells. First, we observed that the percentage of cells in S-phase was increased in HPRT^{low} HSCs but not in early progenitors and mature cells (Fig. 4A, 4B). To further test for cell-cycle dynamics, we performed single-cell proliferation kinetics of HSCs. Indeed, HPRT^{low} HSCs also completed their first division faster than their WT counterpart (Fig. 4C).

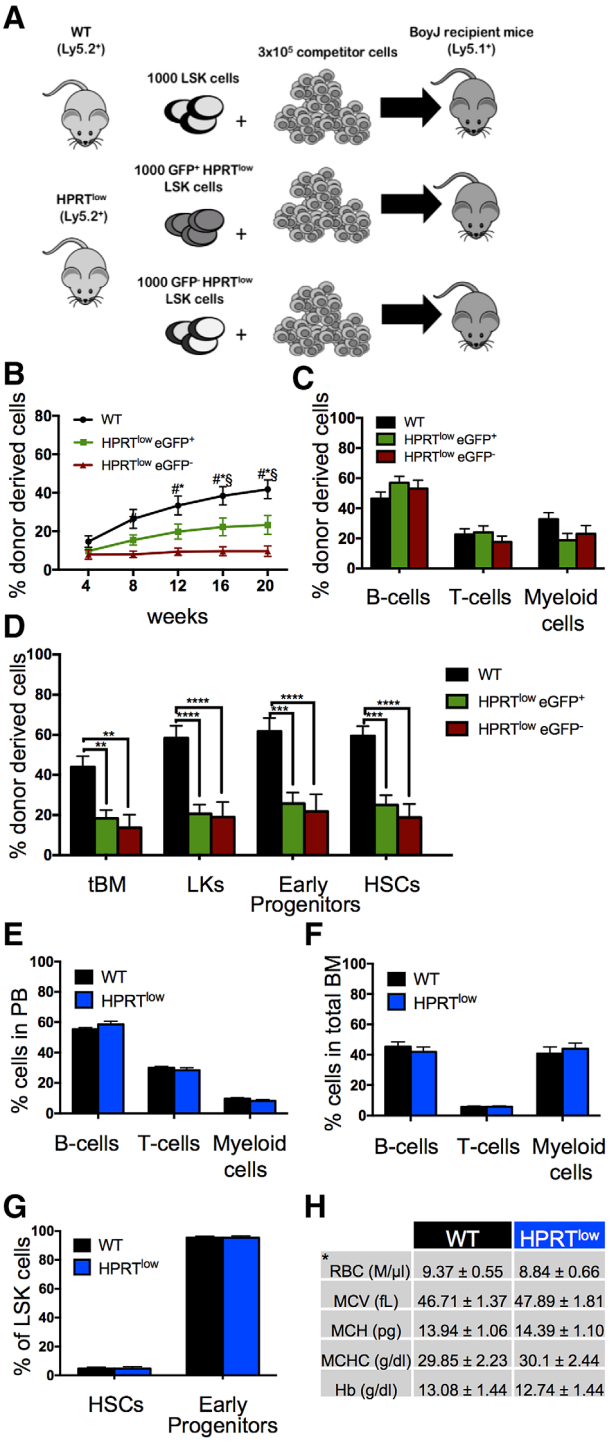

Figure 3. HPRT^{low} hematopoietic stem and progenitor cells (HSPCs) show impaired engraftment. **(A):** Experimental setup: 1,000 Ly5.2$^+$ HSPCs were sorted from wild-type (WT) and HPRT^{low} mice and transplanted together with 3×10^5 Ly5.1$^+$ total bone marrow (BM) cells into lethally irradiated Ly5.1$^+$ mice. **(B):** Chimerism of donor-derived peripheral blood (PB; n = 10–13; two-way ANOVA #$p \le .05$ between WT and eGFP$^-$, $^{\S}p \le .05$ between eGPF$^+$ and eGFP$^-$; *, $p \le .05$ between WT and eGFP$^+$). **(C):** Analysis of donor-derived lineage differentiation after transplantation in PB. B-cells as B220$^+$, T-cells as CD3$^+$, Myeloid cells as Mac-1$^+$, or/and Gr-1$^+$ (n = 10–13; two-way ANOVA). **(d):** Percentage of donor-derived cells in different BM populations after ≥20 weeks (n = 10–11; two-way ANOVA *, $p \le .05$; **, $p \le .01$; ***, $p \le .001$; ****, $p < .0001$). **(E, F):** Analysis of lineage differentiation in steady-state hematopoiesis (E) PB and (F) BM (n = 14; two-way ANOVA). B-cells as B220$^+$, T-cells as CD3$^+$, Myeloid cells as Mac-1$^+$, or/and Gr-1$^+$. **(G):** Percentage of HSCs (Lin$^-$, c-Kit$^+$, Sca-1$^+$, and CD34$^-$) and early progenitors (Lin$^-$, c-Kit$^+$, Sca-1$^+$, and CD34$^+$) within the HSPC population (n = 9; two-way ANOVA). **(H):** Erythrocyte parameters in steady-state hematopoiesis are listed. Shown is the average ± SD. Blood was collected via cardiac puncture after sacrificing WT or HPRT^{low} mice. Blood was collected via cardiac puncture after sacrificing WT or HPRT^{low} mice. Values were obtained with Hemavet905 (mean + SD; n = 14; unpaired t test *, $p \le .05$).

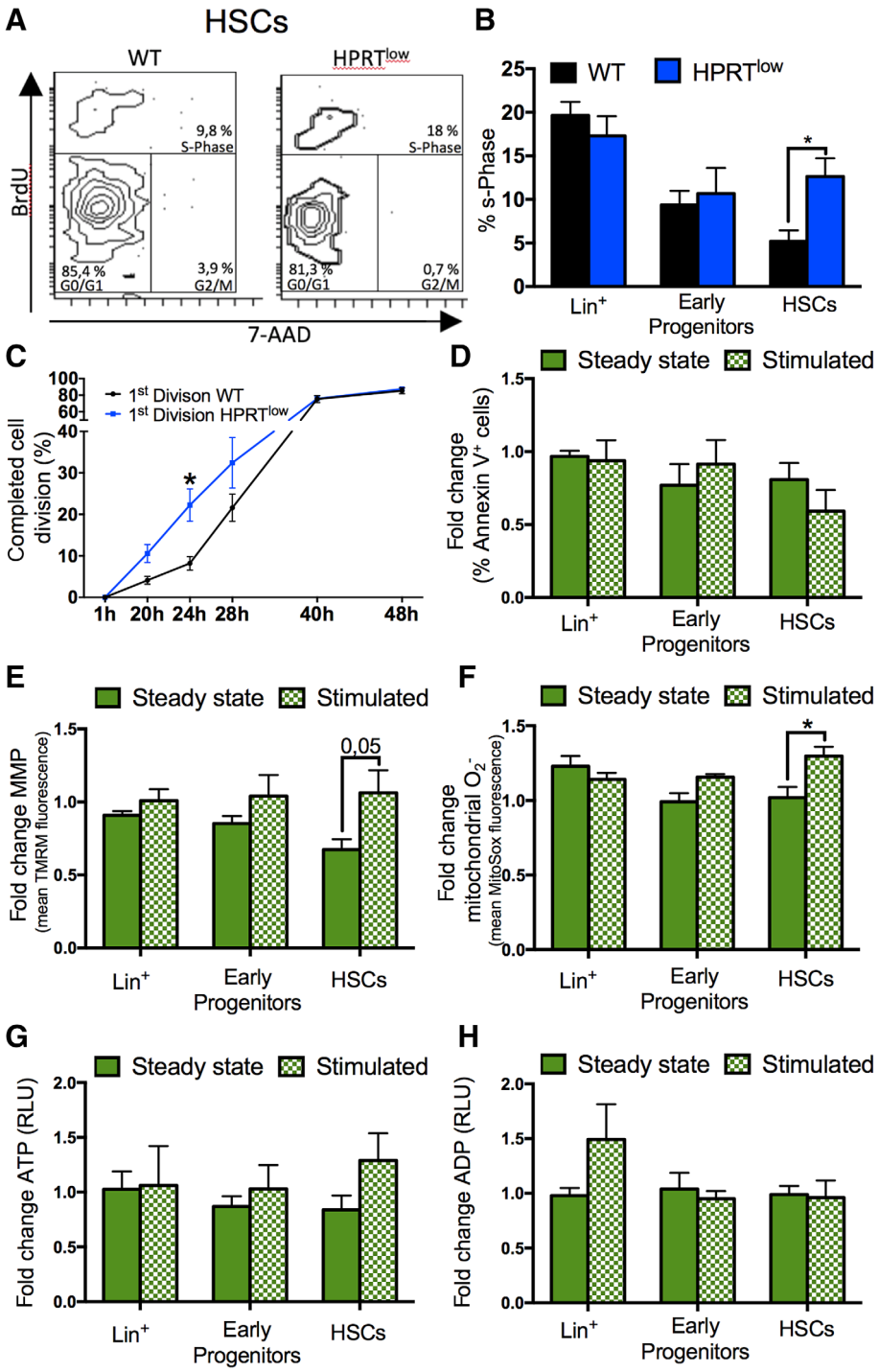

Figure 4. HPRT^{low} hematopoietic stem cells (HSCs) manifest with changes in proliferation kinetics and reduced mitochondrial activity. **(A):** Representative plot of cell-cycle phase analysis of wild-type (WT) and HPRT^{low} HSCs. **(B):** Percentage of cells in S-phase, analyzed by BrdU incorporation (n = 6; two-way ANOVA *, $p \leq .05$). **(C):** Proliferation kinetics of HSCs. Single HSCs of HPRT^{low} or WT origin were observed for 48 hours. Cell divisions were counted (n = 4, [60–70 cells per experiment]; two-way ANOVA, *, $p \leq .05$). **(D):** Fold change of percentage of Annexin V$^+$ cells within the indicated bone marrow (BM) populations in WT and HPRT^{low} mice. Steady state (freshly isolated cells) and stimulated state (48 hours in vitro cytokine stimulation) was normalized to the respective WT measurements (n = 3, 3 mice/n; two-way ANOVA). **(E):** Analysis of mitochondrial membrane potential by TMRM integration. Fold change was calculated by dividing HPRT^{low} mean fluorescence values through the respective WT values. Steady state = freshly isolated or stimulated = 48 hours in vitro stimulated cells (n = 3, 3 mice/n; two-way ANOVA). **(F):** Mitochondrial O_2^- was examined by MitoSox. Illustrated is the fold change of mean MitoSox fluorescence in WT or HPRT^{low} BM populations. Fold change was calculated by dividing through the respective WT measurement. Steady state = freshly isolated or stimulated = 48 hours in vitro stimulated cells (n = 3, 2–3 mice/n, two-way ANOVA *, $p \leq .05$). **(G, H);** Measurement of (G) ATP and (H) ADP amount in 1,000 WT or HPRT^{low} HSCs, early progenitor cells or Lin$^+$ BM cells, detected are the relative luminescence units (RLUs) generated by the conversion of ATP; steady state = freshly isolated and stimulated state = 16 hours in vitro with cytokines. Fold change was calculated by dividing through respective WT (n = 4, 3 mice/n; two-way ANOVA).

The percentage of apoptotic cells, including stem, early progenitor, and differentiated cells, did not differ between WT and HPRT^{low} cells as determined by Annexin V staining (Fig. 4D). A faster progression of HPRT^{low} HSCs through the cell cycle might therefore contribute to their impaired function upon stress.

Additionally, the functional status of mitochondria was investigated, as nucleotide metabolism and energy metabolism might be directly linked. We found that the mitochondrial membrane potential (MMP) was reduced in HPRT^{low} HSCs in steady state (Fig. 4E). Upon activation (cell-cycle initiation in cultivation for 48 hours with cytokines), MMP was similar in HSC from both WT and HPRT^{low} animals (Fig. 4E). The level of mitochondrial superoxide (determined by positive staining with the marker MitoSox) was similar in WT and HPRT^{low} cell populations, whereas, upon activation, there was an increased level in HPRT^{low} compared with WT HSCs (Fig. 4F). Finally, we determined whether low HPRT activity might alter the levels of ATP or ADP in primitive hematopoietic cells, using a sensitive luciferin-based assay (Fig. S5). There was a trend toward a slightly decreased ATP concentration in steady-state HPRT^{low} HSCs, whereas in the stimulated state, ATP levels were slightly elevated (Fig. 4G). The concentration of ADP was equal (Fig. 4H) with the exception of the slight increase of ADP in differentiated cells after stimulation. In summary, HSCs from HPRT^{low} mice show lower MMP in steady state, but elevated levels of mitochondrial superoxide, and a trend toward higher concentrations of ATP in stimulated state, which might in combination also contribute to the impaired function of HSCs upon transplantation.

Discussion

Our enzyme activity assays and the *hprt*/*ppat* gene expression analyses, together with the previously reported finding that PPAT has a lower affinity to PRPP than HPRT [10], suggest that quiescent HSCs favor HPRT-associated purine salvaging over purine de novo synthesis. Interestingly, our data imply that HSCs do not compensate for reduced purine salvaging activity due to low HPRT levels by increasing purine de novo synthesis. Salvaging might thus be the preferred mechanism to sustain purine metabolism in HSCs—even under stress conditions.

HSPCs that show low activity of the purine salvaging pathway caused by low HPRT levels (HPRT^{low}) present with a reduced engraftment upon transplantation (a stress condition), whereas steady-state hematopoiesis was not affected in HPRT^{low} animals. Upon secondary transplantation, we did not detect a further decrease in the reconstitution potential of HPRT^{low} cells over time. This might imply that the self-renewal potential of HPRT^{low} HSCs might not be always and simply intrinsically affected but the defect shows only under distinct stress conditions which were met upon primary transplantation with only a few number of supporting BM cells as competitors compared with the secondary transplants with a high number of supporting BM cells. A difference in cell intrinsic compensation in HPRT$^{-/-}$ cells compared with HPRT^{low} HSCs might also be the underlying reason for the difference in reconstitution potential of HPRT$^{-/-}$ versus HPRT^{low} HSCs (Figs. 3B and Fig. S4). In the complete absence of HPRT in cells of HPRT$^{-/-}$ animals, there was an upregulation of purine nucleotide synthesis [18] and APRT salvaging reported [19], which we did though not observe in HPRT^{low} cells (Fig. 2).

One of the key factors influencing HSC fitness is mitochondrial activity, which was reported to be influenced by an imbalance in purine metabolism [20]. Indeed, we found a reduced MMP abundance in steady state as well as elevated mitochondrial superoxide levels in activated HPRT^{low} HSCs. Both factors in combination are indicative of mitochondrial dysfunction. Interestingly though, the concentration of the prime purine derivatives ATP and ADP was similar in hematopoietic cells from WT and HPRT^{low} mice. These findings match observations made in HPRT deficient neuronal cell lines. Here, the amount of all purine nucleotides was not changed, whereas purine nucleotide binding enzymes and mitochondrial function were rather found to be deregulated [20, 21]. Our data support the finding that a reduction in HPRT and thus purine salvaging does not seem to affect the availability of purine nucleotides in HSCs. This would argue against the theory that HPRT deficient cells are selected against because of reduced DNA synthesis and proliferation of stem cells due to loss of purine nucleotides [22, 23]. In fact, our data show that HPRT^{low} HSCs present with an elevated percentage of cells in S-Phase and faster cell division kinetics, which in combination are indicative of reduced quiescence. We rather propose that the phenotype of HPRT^{low} HSCs is due to an elevated usage and thus activation of the degradation pathway of purines rather than a lack of recycling (Fig. 1A). For example, elevated levels of the purine degradation product hypoxanthine drive cell-cycle progression in *hprt* knockout glioblastoma cells [24]. A dysfunction of mitochondria in HPRT^{low} HSCs might also be attributed to elevated usage of purine degradation. High activity of xanthine oxidase, which is one of the key enzymes important for degradation of purines (Fig. 1A), has been associated with high levels of mitochondrial ROS production [25]. Unfortunately, direct measurements of purine degradation in HSCs are technically not yet possible, given the low number of HSCs per animal. Still, our data support the notion that the balance between purine salvaging and de novo synthesis is not necessary a question of stabilizing the purine nucleotide pool but might be a way of minimizing toxic waste products. Our findings also question whether HPRT negativity might be used as a selection marker for HSCs for downstream transplantation applications in gene therapy protocols [26].

Summary

We have identified the HPRT-associated purine salvaging pathway as a critical contributor to HSC fitness in response to stress. Additionally, we provide evidence that the preference for HPRT-associated purine salvaging is unique for HSCs within primitive hematopoietic stem and progenitor cells. Impaired purine salvaging results in a higher likelihood to enter S-phase and thus in a more active HSC state. We hypothesize that a very critical role of HPRT activity is to reduce the accumulation of toxic purine degradation products to ensure HSCs integrity.

Acknowledgments

The authors thank the Tierforschungszentrum University Ulm and the Animal facility at CCHMC for their help with mouse work and housing of the mice and the FACS core at Ulm University for cell sorting. The authors thank Klaus Schwarz and Erich Schneider for HPRT^{low} and HPRT knockout mice. The authors also thank all the members of the Institute of Molecular Medicine and all members of

the Division of Experimental Hematology and Cancer Biology at Cincinnati Children's for the stimulating discussions and their comments. Work in the laboratory of H.G. was supported by the Deutsche Forschungsgemeinschaft (DFG) SFB 1074 and 1279 and the GRK 1789.

Author Contributions

M.V., H.G.: conception and design; M.V., B.M., K.E.: collection and/or assembly of data; M.V., B.M., A.B., H.G.: data analysis and interpretation; M.V., B.M., A.B., H.G.: manuscript writing; V.S.: provision of study material; H.G.: financial support, administrative support, final approval of manuscript.

Disclosure of Potential Conflicts of Interest

The authors indicated no potential conflicts of interest.

Data Availability Statement

The authors confirm that the data supporting the findings of this study are available within the article or its supplementary materials.

REFERENCES

1 Ito K, Ito K. Metabolism and the control of cell fate decisions and stem cell renewal. Annu Rev Cell Dev Biol 2016;32:399–409.

2 Kim J, Tchernyshyov I, Semenza GL et al. HIF-1-mediated expression of pyruvate dehydrogenase kinase: A metabolic switch required for cellular adaptation to hypoxia. Cell Metab 2006;3:177–185.

3 Takubo K, Goda N, Yamada W et al. Regulation of the HIF-1α level is essential for hematopoietic stem cells. Cell Stem Cell 2010;7:391–402.

4 Simsek T, Kocabas F, Zheng J et al. The distinct metabolic profile of hematopoietic stem cells reflects their location in a hypoxic niche. Cell Stem Cell 2010;7:380–390.

5 Takubo K, Nagamatsu G, Kobayashi CI et al. Regulation of glycolysis by Pdk functions as a metabolic checkpoint for cell cycle quiescence in hematopoietic stem cells. Cell Stem Cell 2013;12:49–61.

6 Shyh-Chang N, Daley GQ, Cantley LC. Stem cell metabolism in tissue development and aging. Development 2013;140:2535–2547.

7 Karigane D, Kobayashi H, Morikawa T et al. p38α activates purine metabolism to initiate hematopoietic stem/progenitor cell cycling in response to stress. Cell Stem Cell 2016;19:192–204.

8 Fasullo M, Endres L. Nucleotide salvage deficiencies, DNA damage and neurodegeneration. Int J Mol Sci 2015;16:9431–9449.

9 Lane AN, Fan TW-M. Regulation of mammalian nucleotide metabolism and biosynthesis. Nucleic Acids Res 2015;43:2466–2485.

10 Natsumeda Y, Prajda N, Donohue JP et al. Enzymic capacities of purine de novo and salvage pathways for nucleotide synthesis in normal and neoplastic tissues. Cancer Res 1984;44:2475–2479.

11 Yamaoka T, Kondo M, Honda S et al. Amidophosphoribosyltransferase limits the rate of cell growth-linked de novo purine biosynthesis in the presence of constant capacity of salvage purine biosynthesis. J Biol Chem 1997;272:17719–17725.

12 Kondo M, Yamaoka T, Honda S et al. The rate of cell growth is regulated by purine biosynthesis via ATP production and G(1) to S phase transition. J Biochem (Tokyo) 2000;128:57–64.

13 Yamaoka T, Yano M, Kondo M et al. Feedback inhibition of amidophosphoribosyltransferase regulates the rate of cell growth via purine nucleotide, DNA, and protein syntheses. J Biol Chem 2001;276:21285–21291.

14 Stout JT, Caskey CT. HPRT: Gene structure, expression, and mutation. Annu Rev Genet 1985;19:127–148.

15 Konecki DS, Brennand J, Fuscoe JC et al. Hypoxanthine-guanine phosphoribosyltransferase genes of mouse and Chinese hamster: Construction and sequence analysis of cDNA recombinants. Nucleic Acids Res 1982;10:6763–6775.

16 Bagger FO, Rapin N, Theilgaard-Mönch K et al. HemaExplorer: A database of mRNA expression profiles in normal and malignant haematopoiesis. Nucleic Acids Res 2013;41:D1034–D1039.

17 Moehrle BM, Nattamai K, Brown A et al. Stem cell specific mechanisms ensure genomic fidelity within HSCs and upon aging of HSCs. Cell Rep 2015;13:2412–2424.

18 Jinnah HA, Page T, Friedmann T. Brain purines in a genetic mouse model of Lesch-Nyhan disease. J Neurochem 1993;60:2036–2045.

19 Wu CL, Melton DW. Production of a model for Lesch-Nyhan syndrome in hypoxanthine phosphoribosyltransferase-deficient mice. Nat Genet 1993;3:235–240.

20 Dammer EB, Göttle M, Duong DM et al. Consequences of impaired purine recycling on the proteome in a cellular model of lesch-nyhan disease. Mol Genet Metab 2015;114:570–579.

21 Göttle M, Burhenne H, Sutcliffe D et al. Purine metabolism during neuronal differentiation: The relevance of purine synthesis and recycling. J Neurochem 2013;127:805–818.

22 McDonald JA, Kelley WN. Lesch-Nyhan syndrome: Absence of the mutant enzyme in erythrocytes of heterozygote for both normal and mutant hypoxanthine-guanine phosphoribosyl transferase. Biochem Genet 1972;6:21–26.

23 Samuel K, Clarke AR, Ansell JD et al. Age-dependent selection against hypoxanthine phosphoribosyl transferase-deficient cells in mouse haematopoiesis. Development 1993;118:859–863.

24 Ma MHY, Stacey NC, Connolly GP. Hypoxanthine impairs morphogenesis and enhances proliferation of a neuroblastoma model of Lesch Nyhan syndrome. J Neurosci Res 2001;63:500–508.

25 Vergeade A, Mulder P, Vendeville C et al. Xanthine oxidase contributes to mitochondrial ros generation in an experimental model of cocaine-induced diastolic dysfunction. J Cardiovasc Pharmacol 2012;60:538–543.

26 Choudhary R, Baturin D, Fosmire S et al. Knockdown of HPRT for selection of genetically modified human hematopoietic progenitor cells. PLoS One 2013;8:e59594.

See www.StemCells.com for supporting information available online.